

## REVIEW OF ACOUSTIC EMISSION CORROSION MONITORING OF PRESTRESSED CONCRETE BRIDGES

**Mohamed K. ElBatanouny, PhD**, Dept. of Civil and Environ. Engineering,  
University of South Carolina, Columbia, SC

**Marwa A. Abdelrahman**, Dept. of Civil and Environ. Engineering,  
University of South Carolina, Columbia, SC

**Paul H. Ziehl, PhD, PE**, Dept. of Civil and Environ. Engineering,  
University of South Carolina, Columbia, SC

### ABSTRACT

*Corrosion of steel reinforcement is a major deterioration mechanism in reinforced concrete structures that has led to highway bridge failures in the recent past. While prestressed and post-tensioned concrete structures offer a natural protection to the reinforcement by limiting crack development, the high stresses in prestressing strands and their geometry facilitates crevice corrosion which accelerates corrosion deterioration and may increase the risk of sudden failure. Traditional methods for corrosion detection, such as visual inspection and electrochemical measurements, are local, time consuming and may not be feasible in post-tensioned concrete structures. This study summarizes recent efforts that utilize the acoustic emission technique for corrosion detection in prestressed and post-tensioned concrete structures. Acoustic emission is sensitive to ongoing damage and can detect it on both the micro- and macro-level. The method is non-intrusive and can enable global assessment of the structural condition. The methodology is reviewed and the results of accelerated corrosion experiments on specimens with different sizes and configurations are reported. In these studies, acoustic emission results are validated using electrochemical results and micro-graphs from scanning electron microscopy. A newly developed acoustic emission based corrosion classification chart is also presented.*

**Keywords:** Corrosion, Prestressed concrete, Post-tensioned concrete, Acoustic emission

## INTRODUCTION

Since the construction of the Walnut Lane Memorial Bridge in 1951, prestressed (PC) and post-tensioned (PT) concrete have been widely used in the construction industry in the United States. These construction types offer several advantages over passively reinforced concrete (RC) as they have smaller section sizes, higher span-to-depth ratio, higher strength-to-weight ratio, and smaller deflections. As of today, 24.4% of the bridges in the United States have been built using PC<sup>1</sup>. While most of the PC and PT concrete structures have had an exemplary performance, two collapses in the United States in the past 15 years occurred in PC bridges; Lowes Motor Speedway in Concord, NC, 2000, and the I-70 Overpass in South Strabane, PA, 2004. In both incidents, evidence of corrosion damage was found in the prestressing strands of the structure. Corrosion was also responsible for the suspension of segmental PT bridges in the United Kingdom after the failure of the Ynys-y-Gwas Bridge in 1985<sup>2</sup>.

Corrosion of reinforcement is a major cause for deterioration of RC structures in coastal areas or areas where de-icing salts are used<sup>3</sup>. In spite of the natural protection concrete provides for the steel reinforcement to resist corrosion, due to formation of protecting passive oxide film around the steel as a result of the high alkalinity of concrete; chlorides can infiltrate through concrete cracks to break the passive film and initiates corrosion in reinforcing steel<sup>4</sup>. The design methodology of PC offers an additional protection to the prestressing strands as it inhibits formation of cracks, for example Class U PC in ACI 318-11<sup>5</sup>. This makes PC structures more resistive to corrosion damage as compared to RC structures. However, due to their geometry, prestressing strands are more vulnerable to localized corrosion forms, such as pitting and crevice corrosion, than reinforcing bars. Furthermore, the high stress state of prestressing strands and their lower deformability leads to more brittle failure than reinforcing bars. This makes corrosion damage, if exists, more critical in PC structures as it leads to sudden failures.



Fig.1 Corrosion process in concrete (<http://concrete-forum.com/>)

Chloride induced corrosion reduces the mechanical strength of steel reinforcement and corrosion product exerts stress into the concrete structure producing cracks that deteriorate the steel-concrete bond, which directly affects the serviceability performance. When steel starts to corrode, a gradual decrease of its diameter is produced, together with the generation of an oxide of six to ten times higher volume than that of steel<sup>6</sup>. The corrosion process in

then accelerated by the presence of cracks which increases the rate of chloride infiltration. Corrosion affects the durability of concrete structures and decreases its service life by: a) reducing the cross sectional area of the steel strands minimizing their ductility and increasing stress concentrations at the reinforcement interface<sup>7</sup>, and b) degrading the integrity of the surrounding concrete<sup>8</sup>. Fig. 1 shows a schematic of the corrosion process in concrete.

Currently, the main methods used for corrosion detection are visual inspection and electrochemical measurements. The former can only detect corrosion if signs of corrosion damage are visible on the concrete in the form of cracking or concrete spalling. At this point, the corrosion process has usually reached a severe degree where intensive repair or replacement of the affected structure is required. Electrochemical techniques can detect the corrosion process at an early stage; however, these methods require a physical connection to the steel and can only give the measurement in one spot which makes them local and intrusive. In addition, a long period of time is needed to generate a corrosion map of the structure.

This paper summarizes the current progress at the University of South Carolina in using the acoustic emission (AE) technique for detection and classification of corrosion damage. AE is a passive structural health monitoring (SHM) technique with an ability to detect stress waves released by cracking long before they are visible (micro-cracking). Recent advances in AE equipment have paved the way for implementation of this method for damage detection in concrete structures. AE based methods for corrosion detection are presented along with the recently developed chart for corrosion classification in PC structures.

## **CORROSION DETECTION ELECTROCHEMICAL METHODS**

### **HALF-CELL POTENTIAL**

Half-cell potential measurements (HCP) are widely used for corrosion detection. The method is available in an ASTM standard (ASTM C876). The methodology of this method consists of comparing the corrosion potential of the reinforcing steel with a reference potential and estimating the probability of corrosion based on the potential reading. The reference electrode, copper-copper sulfate (Cu-CuSO<sub>4</sub>) or silver chloride (AgCl), is connected to a positive terminal and the reinforcement is connected to a negative terminal of a voltmeter. This establishes a potential difference which offers information related to structural decay. The reference electrode should be placed on the concrete surface near the measured values stabilized. Table 1 shows the ASTM C876 criteria for corrosion detection using half-cell potential measurements<sup>9</sup>.

Table 1. ASTM corrosion for Cu-CuSO<sub>4</sub> and AgCl reference electrode<sup>10</sup>

Potential Against Cu-CuSO <sub>4</sub> Electrode	Potential Against AgCl Electrode	Corrosion Condition
> -200 mV	> -100 mV	Low Risk (10% probability of corrosion)
-200 to -350 mV	-100 to -250 mV	Intermediate corrosion risk
< -350 mV	< -250 mV	High Corrosion risk (90% probability)
< -500 mV	< -400 mV	Severe Corrosion Damage

## LINEAR POLARIZATION RESISTANCE

Linear Polarization Resistance (LPR) measurements are used to measure the polarization resistance ( $R_p$ ), corrosion current ( $i_{corr}$ ), and corrosion rate of the steel. Andarde et al. 1990<sup>11</sup> also used this method to classify corrosion damage based on the measured corrosion rate. The LPR measurements are conducted using a potentiostat three-electrode principle. The unit functions by maintaining the potential of a working electrode at a constant level with respect to a reference electrode while adjusting the current at a counter electrode<sup>12</sup>. A Linear Polarization Resistance (LPR) sweep is then performed by applying a scanning potential of  $\pm 20$  mV around the potential difference as measured between the reference and the working electrode ( $E_{corr}$ ). The resulting current that passes between the working and the counter electrode is then measured ( $i_{corr}$ )<sup>13</sup>.

The polarization resistance,  $R_p$ , is the slope of the line formed between  $E_{corr}$  and resulting  $i_{corr}$ . The polarization resistance can be calculated using Equation 1 where  $R_p$  is the polarization resistance,  $\Omega\text{-cm}^2$ ;  $\Delta E$  is the change in applied potential relative to corrosion potential  $E_{corr}$ , mV; and  $\Delta i$  is the current response to applied potential spectrum, mA.  $i_{corr}$  is the corrosion current,  $\mu\text{A}$ ;  $b_a$ ,  $b_c$  are the anodic and cathodic Tafel slopes respectively, mV.

$$R_p = \frac{\Delta E}{\Delta i} = \frac{b_a \times b_c}{2.303 \times i_{corr} (b_a + b_c)} \quad (1)$$

With the polarization resistance known from the LPR sweep, the corrosion current ( $i_{corr}$ ) can be calculated from Equation 1. Equation 2 is then used to calculate corrosion rate (CR) in milli-inch per year (mpy). In Equation 2, EW is the equivalent weight of iron, 27.92 g; A is the surface area of the anode,  $\text{cm}^2$ ; and  $d$  is the density of iron,  $7.8 \text{ g/cm}^3$ .

$$CR = \frac{0.13 \times i_{corr} \times EW}{A \times d} \quad (2)$$

## ACOUSTIC EMISSION

### BACKGROUND

Acoustic emission (AE) is the term used to define transient stress waves emitted from sudden release energy<sup>14</sup> due to a deformation in the monitored material, such as crack formation or growth<sup>15,16</sup>. AE is a passive SHM technique which does not need excitation or human intervention after the sensors are connected to the data acquisition system. The waveform of each AE signal (AE hit) can be used to calculate different parameters such as amplitude, duration, counts, rise time, absolute energy, and signal strength along with different frequency parameters as shown in Figure 2. In this paper, signal strength (the measured area of the rectified AE signal with units proportional to volt seconds [pVs]) is used for corrosion detection.

AE has the ability to locate cracks using triangulation. The location of each AE source event (AE signals that are detected by at least two sensors) can be determined using the arrival times of the compression waves. Due to the extreme sensitivity of the method, data filtering is a crucial step in AE analysis. The main source of noise in the AE data in laboratory testing is wave reflections. Duration-amplitude filters (D-A filters), also known as Swansong II filters<sup>17</sup>, and rise time-amplitude filters (R-A filters) are widely used for rejection of wave reflections from AE data. These filters are usually developed through visual inspection of waveforms related to noise, and determining the relation between AE parameters for these hits. Literature indicates that crack maps can be produced with high reliability if proper data filters were used<sup>18-20</sup>.

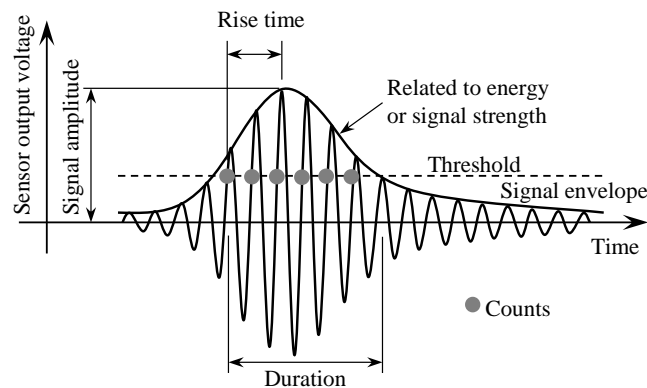


Fig.2 Schematic of Acoustic Emission waveform

### AE CORROSION DETECTION

The mechanisms that enable correlation between AE data and corrosion rate are: a) accumulation of chlorides and breakdown of the passive film<sup>21,22</sup> and b) the micro-cracking of the concrete that occurs due to the expansive nature of the corrosion products<sup>3,13</sup>. The primary advantage of AE monitoring is its unique ability to detect and quantify the micro-cracking process as it occurs, making it an extremely sensitive monitoring method. Later

stages of corrosion damage, such as visible surface cracking, are also easily detected and quantified.

Corrosion detection using AE has been researched since the 1980's<sup>23,24</sup>. However, most of the studies focused on passively reinforced concrete as opposed to prestressed concrete. The main focus of earlier studies was to investigate the ability of AE to detect corrosion initiation. Literature indicates that AE parameters such as number of AE hits and/or events have the ability to detect corrosion as well as to detect changes in the rate of the corrosion process<sup>6,25,26</sup>. Recent studies also investigated the use of AE based condition assessment such as Simplified Green's functions for moment tensor analysis (SiGMA) and  $b$ -value<sup>27,28</sup>.

## CORROSION CLASSIFICATION IN PC STRUCTURES

Although the mechanism of corrosion activity in RC and PC is similar, the manufacturing process and shape of prestressing strands facilitates corrosion initiation at a lower chloride concentration as compared to steel rebars<sup>29</sup>. Most of the earlier studies can detect corrosion damage but do not directly relate AE activity to the rate of corrosion and in determining the extent of corrosion. This section summarizes recent efforts at the University of South Carolina for corrosion detection and classification of prestressing strands in PC and PT specimens with different scales and durations of corrosion exposure. In these studies, ½ in. (12.7 mm) seven wire low-relaxation prestressing strands were used in all specimens. AE R6i sensors (peak resonance at approximately 55 kHz, with integral 40 dB<sub>AE</sub> [referred to as dB for simplicity] pre-amplification) were used to monitor corrosion in all the studies. It is noted that all the AE data shown is filtered. The main filters used are duration-amplitude (D-A) filters which are based on inspection of AE signals to differentiate noise from genuine AE data. The limits used in the D-A filters from ElBatanouny et al. 2014<sup>3</sup> are shown in Table 2. For more information regarding the filtration techniques please refer to the referenced manuscripts<sup>3,30,31</sup>.

Table 1. AE Duration-Amplitude data filter<sup>3</sup>

Rejection limits		Rejection limits		Rejection limits	
Amp, dB	Dur, $\mu$ s	Amp, dB	Dur, $\mu$ s	Amp, dB	Dur, $\mu$ s
40-42	>400	50-52	>1,500	60-65	>4,500
42-44	>600	52-54	>2,000	65-70	>6,500
44-46	>800	54-56	>2,500	70-75	>7,500
46-48	> 1,000	56-58	> 3,000	75-80	> 9,000
48-50	>1,200	58-60	>3,500	90-100	>10,000

## SMALL SCALE SPECIMENS

A total of twenty specimens were tested under an accelerated corrosion test setup. The specimens were reinforced with an embedded  $\frac{1}{2}$  inch diameter prestressing strand; dimensions of each specimen were 4.5 in x 4.5 in x 20 in. (114 x 114 x 1270 mm). The test matrix included eleven precracked specimens and nine pristine specimens to evaluate the effect of cracks on AE attenuation. Specimens were immersed in a tank filled with a 3% NaCl solution at room temperature to a level 0.25 inch (7 mm) below the reinforcing strand. A copper plate with the same length of the specimens was placed below each specimen to serve as the cathode.

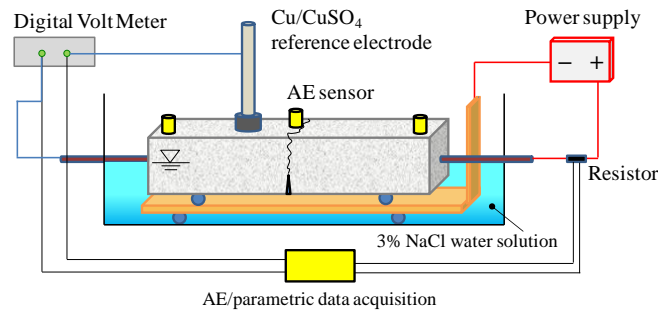


Fig. 3 Schematic of the accelerated corrosion setup<sup>30</sup>

Accelerating the corrosion process was established by forming a galvanic cell using a rectifier to impress a direct external current to the specimens. The current that flows between the dissimilar metals controls the degree of corrosion activity in the cell. The rectifier was connected between the copper plate (cathode) and the prestressing strand (anode). Figure 3 shows a diagram of the corrosion cell for a single cracked specimen placed in the test vessel<sup>30</sup>.

The results showed that stresses induced by volume expansion resulted in dense AE that was correlated to the onset of corrosion and nucleation of cracks as shown in Figure 4. Comparing acoustic emission data with electrochemical HCP measurements showed that the cumulative signal strength relates well with potential variations as shown in Figure 5. It also allowed discrimination between different corrosion stages. The magnitude of the slope in the cumulative signal strength (CSS) versus time curve was able to portray the depassivation process and onset of corrosion as corroborated by HCP. This shows that AE is capable of detecting and discriminating between early corrosion stages while mimicking the behavior of resistivity changes in the concrete.

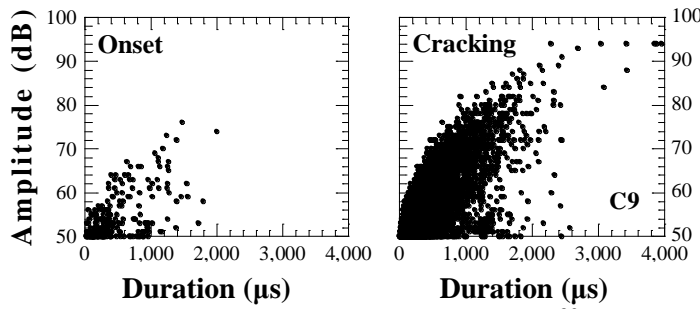


Fig. 4 Amplitude (dB) vs. duration ( $\mu\text{s}$ ) plot<sup>30</sup>

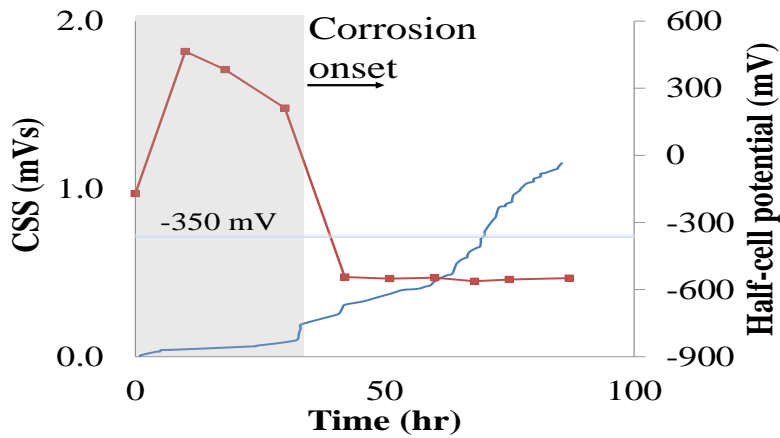


Fig. 5 Cumulative signal strength and half-cell potential versus time

Source location based on AE data enabled the accurate detection of events as a result of passivity breakdown along the reinforcement and debonding<sup>30,31</sup>. Figure 6 shows the source location results for a precracked specimen. As seen in the figure, most of the AE activity concentrated near to the crack where corrosion is predicted to take place as a result of chlorides accessibility in this region (no AE activity was detected at the exact crack location as it is already formed). At the conclusion of the test, the specimens were taken apart and the strand was removed for visual inspection of corrosion. The strand was then cleaned and reweighed to measure the steel mass loss as detailed in Mangual et al. 2013<sup>30</sup>. As shown in Figure 7, heavy corrosion damage, in terms of formation of longitudinal and tangential cracks, was observed in some of the specimens.

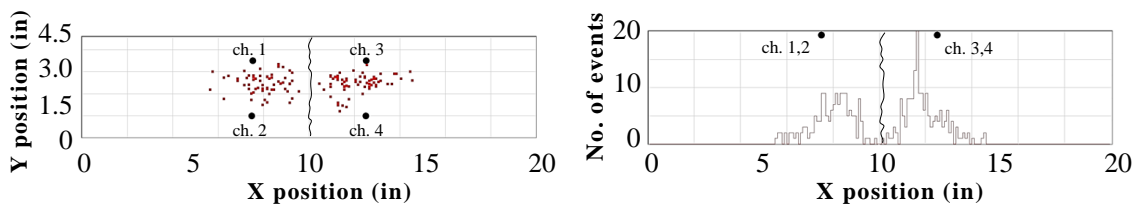


Fig. 6 Source location and number of events for a precracked specimen

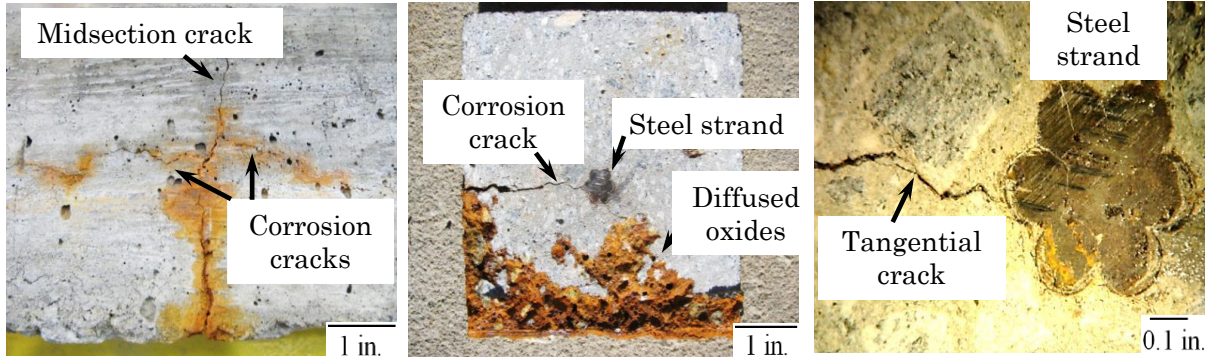


Fig. 7 Corrosion damage in steel and concrete

ElBatanouny et al. 2011 proposed that AE Intensity Analysis can be used to classify corrosion damage<sup>13</sup>. The method was first proposed by Fowler et al. 1989<sup>17</sup> to quantify damage in FRP vessels and tanks by calculating two parameters: historic index,  $H(t)$ , and severity,  $S_r$ . Historic index is a form of trend analysis that measured the rate of change in the cumulative signal strength while severity is the average of certain number of hits (50 hits) with the highest signal strength. The increase in these parameters can be related to accumulation of damage. Historic index and severity can be calculated using Equations 3 and 4 where:  $N$  is number of hits up to a time ( $t$ ),  $S_{oi}$  is the signal strength of the  $i$ -th event, and  $K$  is empirically derived factor that varies with number of hits. In this study, the value of  $K$  was selected to be: a) N/A if  $N \leq 50$ , b)  $K = N - 30$  if  $51 \leq N \leq 200$ , c)  $K = 0.85N$  if  $201 \leq N \leq 500$ , and d)  $K = N - 75$  if  $N \geq 501$  (Nair and Cai 2010).

$$H(t) = \frac{N}{N - K} \frac{\sum_{i=k+1}^N S_{oi}}{\sum_{i=1}^N S_{oi}} \quad (3)$$

$$S_r = \frac{1}{50} \sum_{i=1}^{50} S_{oi} \quad (4)$$

Intensity Analysis results were correlated with HCP measurements and measured sectional mass loss yielding two AE based corrosion classification charts for precracked and uncracked specimens as shown in Figure 8. For precracked specimens the chart divides the corrosion damage into four categories as illustrated in Mangual et al. 2013<sup>30</sup> as follows: A) No damage: at this level the steel is still in the passive condition and no corrosion damage occurred, b) Depassivation: at this level corrosion has just initiated with sectional mass loss less than 15%, c) Cracking: refers to the level at which cracks due to corrosion started to form and the sectional mass loss is less than 21%, and d) Severe damage: more cracks form and the sectional mass loss exceeds 21%. For pristine specimens, specimens in which depassivation was absent laid in region A of the intensity analysis grading chart, whereas depassivated specimens lay in the B region<sup>31</sup>. These charts enable early detection of corrosion and classification of corrosion damage. Such charts also could extend the use of AE to personnel

that are less acquainted with the method to perform damage evaluation without the need to send the collected data to AE specialist. It is noted that these figures includes uncertainties associated with AE monitoring which should be studied and quantified in future studies.

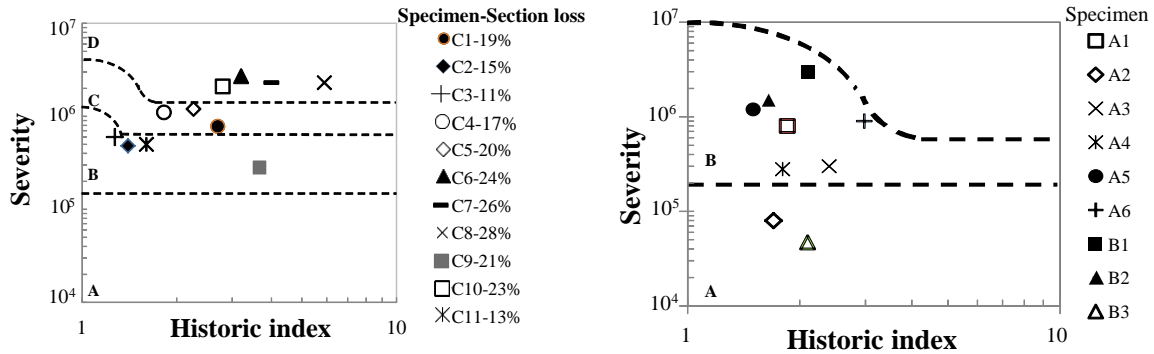


Fig. 8 AE based corrosion classification charts for (left) precracked specimens and (right) pristine specimens<sup>30,31</sup>

MEDIUM SCALE SPECIMENS

Long term corrosion tests were performed on medium scale PC beams to provide better representation of actual environments for corrosion. The corrosion was accelerated using 3 day wet/4 day dry cycles with a 3% NaCl solution as shown in Figure 9. Each beam was reinforced with two ½ in. (12.7 mm) prestressing strands located in the compression zone and measured 16 ft. 4 in. in length (4.98 m). The beams were T-shaped with a total height of 15 in. (380 mm), a web thickness of 6 in. (150 mm), and a flange width and depth of 24 in. (610 mm) and 3 in. (75 mm), respectively. The test included three specimens where two were precracked to 0.016 in. (0.4 mm), specimen CC-0.4, and 0.032 in. (0.8 mm), specimen CC-0.8, while the last specimen was pristine. The specimens were continuously monitored by AE for 140 days. No corrosion damage was detected in the pristine specimen from any method due to the limited ability of chlorides to penetrate through concrete subjected to prestressing force.

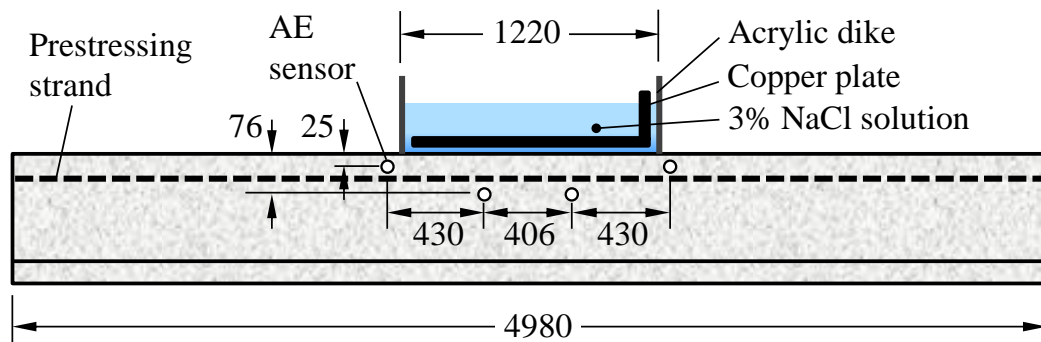


Fig. 9 Corrosion test setup and AE sensor layout (in mm; 1 in. = 25.4 mm)

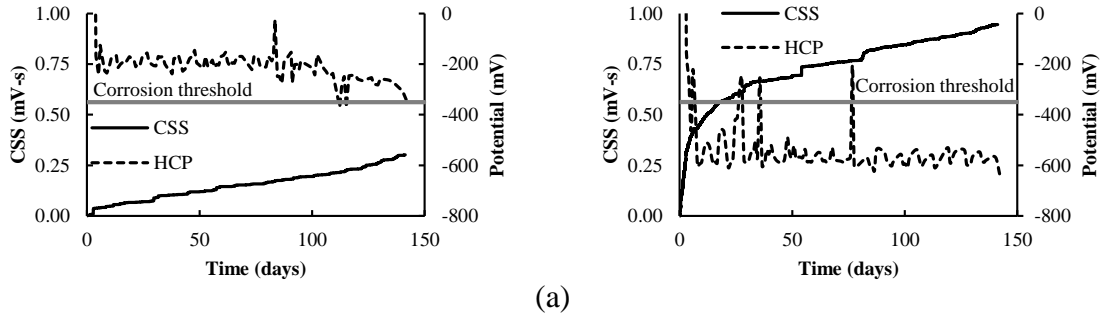


Fig. 10 Cumulative signal strength and half-cell potential versus time. (a) Specimen precracked crack width (a) 0.016 in. (0.4 mm), specimen CC-0.4 and (b) 0.032 in. (0.8 mm), specimen CC-0.8<sup>3</sup>

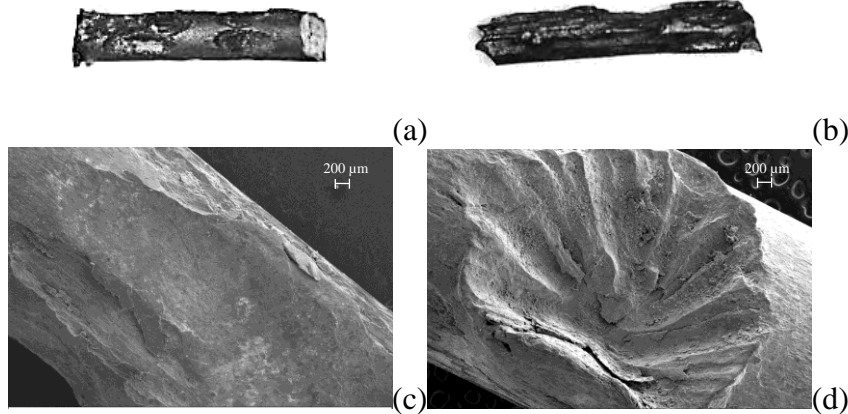


Fig. 11 Photographs showing pitting corrosion: (a-b) specimens CC-0.4 and CC-0.8, respectively, and (c-d) SEM micrographs specimens CC-0.4 and CC-0.8, respectively. (1 in. = 25.4 mm)<sup>3</sup>

The results of the precracked specimens showed that the AE parameter CSS is able to detect corrosion with a higher sensitivity than HCP. As shown in Figure 10, HCP for specimen CC-0.8 showed that corrosion initiated within the first week of testing which agreed with CSS results which showed high rate of corrosion activity. For specimen CC-0.4, HCP results only approached the corrosion threshold towards the end of the test while AE was showing a steady increase in the AE activity illustrating that corrosion is occurring. To further investigate the corrosion activity, LPR measurements were also taken. Based on Andrade et al. 1990 classification, LPR results showed that CC-0.4 had a moderate corrosion rate while CC-0.8 had a high corrosion rate. This agrees with the AE results where the rate of AE activity for CC-0.8 was higher than that of CC-0.4. Visual inspection of damaged prestressing strands showed a clear evidence of pitting (localized) corrosion in both specimens as shown in Figure 11. This corrosion type leads to a significant reduction in the residual capacity of the specimens. Crack width is a significant factor in the formation and intensity of pitting in terms of pit depth. Load testing of the beams at the conclusion of the test showed a reduction in the capacity of the beams where corrosion was detected by AE as compared to the pristine

specimen where no corrosion was detected. This indicated that AE has the ability to detect corrosion before a reduction in the strength of the structure occurs<sup>3</sup>. Therefore, adapting this method for real-time corrosion monitoring can reduce, if not eliminate, the risk of sudden failure as a result of corrosion damage<sup>3</sup>.

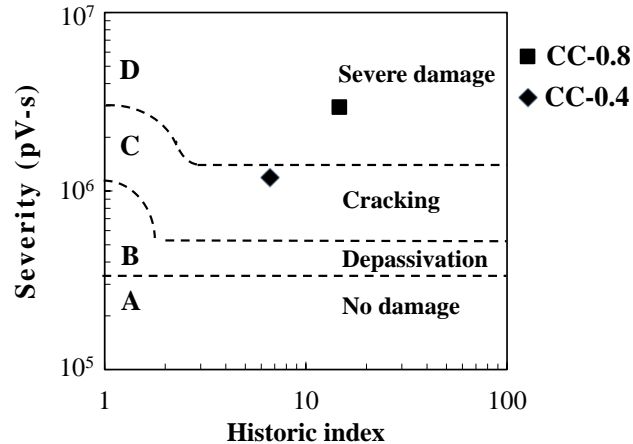


Fig. 12 Corrosion intensity analysis results for cracked specimens<sup>3</sup>

Intensity Analysis was performed on the cracked specimens using the limits set in the small scale specimens study as shown in Figure 12. The results showed that AE Intensity Analysis can enable the detection and classification of corrosion damage. This is true for small and medium scale specimens illustrating that the method may be independent of specimen size and duration of exposure. These results were also compared with LPR results and had a good agreement.

## SUMMARY AND RECOMMENDATIONS

The feasibility of acoustic emission to detect corrosion was evaluated by comparing the AE results to electrochemical methods, sectional mass loss, and visual evidence of corrosion damage. The AE parameter of signal strength was found to detect the initiation of corrosion prior to HCP measurement. The method can be effectively used in places where there is no provision for electrochemical measurements. AE based Intensity Analysis charts can enable the detection and classification of corrosion damage using empirical limits for corrosion levels. This chart classifies corrosion damage in specimens with different sizes and exposure times showing that it may be independent of size and duration.

Unlike some electrochemical techniques, the proposed AE corrosion classification charts have the ability to detect and quantify corrosion damage at early stages. This enables the development of acoustic emission into a damage quantification tool for maintenance prioritization because significant damage (such as macro-cracking and spalling) is not required for detection. The proposed chart can also be used to estimate safe remaining

service life as it is linked to cross sectional mass loss results. However, the uncertainties associated with the relation between AE and mass loss should be quantified prior to full implementation.

AE is a non-intrusive method and has the ability to detect damaged areas through source triangulation. The high sensitivity of the method enables it to perform global assessment of the structure. The method is currently deployable in elements such as piles and foundations. For superstructures, a method to separate AE data from corrosion and that from other sources such as service loading should be developed.

AE is suitable for field applications as wireless AE equipment is commercially available with low-power requirements and can utilize solar or wind power to operate. More studies should be conducted on the applicability of the developed charts for field applications. Uncertainties related to noise rejection, AE wave speed, and signal attenuation in the field should also be investigated.

## ACKNOWLEDGEMENTS

This work is performed under the support of the U.S. Department of Commerce, National Institute of Standards and Technology, Technology Innovation Program, Cooperative Agreement Number 70NANB9H9007.

## REFERENCES

1. National Bridge Inventory (NBI), , “Tables of Frequently Requested NBI Information: Deficient Bridges by State and Highway System,” *Federal Highway Administration (FHWA)*, 2013.
2. Trejo, D., Pillai, R.G., Hueste, M.B., and Reinschmidt, K.F., “Parameters Influencing Corrosion and Tension Capacity of Post-Tensioning Strands,” *ACI Materials Journal*, V. 106, No. 2, March 2009, pp.144-153.
3. ElBatanouny, M.K., Mangual, J., Ziehl, P., and Matta, F., “Early Corrosion Detection in Prestressed Concrete Girders Using Acoustic Emission,” *Journal of Materials in Civil Engineering*, V. 26, No. 3, March 2014, pp. 504–511.
4. Austin, S., Lyons, R., and Ing. M., “Electrochemical Behavior of Steel-Reinforced Concrete during Accelerated Corrosion Testing,” *Corrosion*, V. 60, No. 2, 2004, pp. 203-212.
5. ACI 318-11, “Building Code Requirements for Structural Concrete,” *ACI Committee 318*, Farmington Hills, MI, 2011, pp. 503.
6. Li, Z., Li, F., Zdunek, A., Landis, E., and Shah, S.P., “Application of Acoustic Emission Technique to Detection of Reinforcing Steel Corrosion in Concrete,” *ACI Materials Journal*, V. 95, No. 1, January 1998, pp. 68-76.

7. Yoon, D., Weiss, W., and Shah, S., "Assessing Damage in Corroded Reinforced Concrete Using Acoustic Emission," *Journal of Engineering Mechanics*, V. 126, No. 3, 2000, pp. 273-283.
8. Jaffer, S., and Hansson, C., "Chloride-Induced Corrosion Products of Steel in Cracked-Concrete Subjected to Different Loading Conditions," *Cement and Concrete Research*, V. 39, 2009, pp. 116-125.
9. ASTM C876, "Standard Test Method for Half-Cell Potentials of Uncoated Reinforcing Steel in Concrete," *American Standard for Testing and Materials*, 2009, pp. 1-7.
10. Broomfield, J. P., "Corrosion of Steel in Concrete," Second Edition, 2007.
11. Andrade, C., Alonso, M.C., and Gonzalez, J.A., "An Initial Effort to Use Corrosion Rate Measurements for Estimating Rebar Durability Corrosion Rates of Steel in Concrete," *ASTM STP 1065*, N.S. Berke et al. editors, ASTM, Philadelphia, 1990, pp. 29-37.
12. ASTM G59 (1997-Reapproved 2009), "Standard Test Method for Conducting Potentiodynamic Polarization Resistance Measurements," *American Standard for Testing and Materials*, pp. 1-4.
13. ElBatanouny, M., Mangual, J., Ziehl, P., and Matta, F., "Corrosion Intensity Classification in Prestressed Concrete using Acoustic Emission Technique," *Proc. American Society for Nondestructive Testing (ASNT) Fall Conference and Quality Testing Show 2011*, Palm Springs, CA, 2011, pp. 8.
14. ASTM E1316-13c, "Standard Terminology for Nondestructive Examinations," *American Standard for Testing and Materials*, 2013, pp.1-38.
15. Ziehl, P., "Applications of Acoustic Emission Evaluation for Civil Infrastructure," *Proc. SPIE Smart Structures NDE*, San Diego, CA, 2008, pp. 9.
16. Pollock, A.A., "Classical Wave Theory in Practical AE Testing," *Progress in AE III, Proceedings of the 8th International AE Symposium*, Japanese Society for Nondestructive Testing, 1986, pp. 708-721.
17. Fowler, T.J., Blessing, J., Conlisk, P., and Swanson, T., "The MONPAC Procedure," *Journal of Acoustic Emission*, V. 8, No. 3, 1989, pp. 1-8.
18. Abdelrahman, M., ElBatanouny, M.K., and Ziehl, P., "Acoustic Emission Based Damage Assessment Method for Prestressed Concrete Structures: Modified Index of Damage," *Engineering Structures*, V. 60, February 2014, pp. 258–264.
19. ElBatanouny, M.K., Ziehl, P., Larosche, A., Mangual, J., Matta, F., and Nanni, A., "Acoustic Emission Monitoring for Assessment of Prestressed Concrete Beams," *Construction and Building Materials*, V. 58, May 2014, pp. 46–53.
20. ElBatanouny, M.K., Larosche, A., Mazzoleni, P., Ziehl, P., Matta, F., and Zappa, M., "Identification of Cracking Mechanisms in Scaled FRP Reinforced Concrete Beams using Acoustic Emission," *Experimental Mechanics*, V. 54, No.1, January 2014, pp. 69-82.
21. Perrin, M., Gaillet, L., Tessier, C., and Idrissi, H., "Hydrogen Embrittlement of Prestressing Cables," *Corrosion Science*, V. 52, June 2010, pp. 1915–1926.
22. Prateepasen, A., and Jirarungsatian, C., "Implementation of Acoustic Emission Source Recognition for Corrosion Severity Prediction," *Corrosion*, V. 67, No. 5, May 2011, pp. 11.
23. Weng, M.S., Dunn, S.E., Hartt, W.H., and Brown, R.P., "Application of Acoustic Emission to Detection of Reinforcing Steel Corrosion in Concrete," *Corrosion*, V. 38, No. 1, January 1982, pp. 9-14.

24. Abdelrahman, M., "Assessment of Damage in Concrete Structures Using Acoustic Emission," *Master Thesis*, University of South Carolina, 2013, pp. 146.
25. Zdunek, A.D., Prine, D.W., Li, Z., Landis, E., and Shah, S., "Early Detection of Steel rebar Corrosion by Acoustic Emission Monitoring," *Paper No. 547 presented at CORROSION95*, the NACE International Annual Conference and Corrosion, 1995, pp. 9.
26. Idrissi, H., and Limam, A., "Study and Characterization by Acoustic Emission and Electrochemical Measurements of Concrete Deterioration Caused by Reinforcement Steel Corrosion," *NDT & E International*, V. 36, No. 8, December 2003, pp. 563-569.
27. Farid Uddin, A.K.M., Numata, K., Shimasaki, J., Shigeishi, M., and Ohtsu, M., "Mechanisms of Crack Propagation due to Corrosion of Reinforcement in Concrete by AE-SiGMA and BEM," *Construction and Building Materials*, V. 18, No. 3, April 2004, pp. 181-188.
28. Ohtsu, M., and Tomoda, Y., "Phenomenological Model of Corrosion Process in Reinforced Concrete Identified by Acoustic Emission," *ACI Materials Journal*, V. 105, No. 2, March 2008, pp. 194-199.
29. Moser, R.D., Singh, P. M., Kahn, L.F., and Kurtis, K.E., "Chloride-Induced Corrosion of Prestressing Steels Considering Crevice Effects and Surface Imperfections," *Corrosion*, V. 67, No. 6, pp. 065001:1-14.
30. Mangual, J., ElBatanouny, M.K., Ziehl, P., and Matta, F. (2013). "Acoustic-Emission-Based Characterization of Corrosion Damage in Cracked Concrete with Prestressing Strand," *ACI Materials Journal*, V. 110, No. 1, January-February 2013, pp.89-98.
31. Mangual, J., ElBatanouny, M.K., Ziehl, P., and Matta, F., "Corrosion Damage Quantification of Prestressing Strands Using Acoustic Emission," *Journal of Materials in Civil Engineering*, V. 25, No. 9, September 2013, pp. 1326–1334.